Photoemission Studies of CdTe*†

J. L. SHAY‡ AND W. E. SPICER
Stanford Electronics Laboratories, Stanford University, Stanford, California
(Received 31 March 1967)

By correlating structure in the CdTe energy distributions of the photoemitted electrons with structure in the optical data, we determine the absolute energies of the initial and final states for the transitions associated with peaks in the reflectivity at 6.8 and 7.6 eV and shoulders at 5.8 and 8.7 eV. It is shown that the structure in the energy distributions results from a mixture of direct and nondirect transitions. The direct transitions allow us to locate the conduction-band states Γ_{15} and Γ_1 at 5.8 and 8.7 eV above the valence-band maximum, the uppermost valence band along the zone edge W to K at -1.3 eV, and the second conduction band along the zone edge W to K at 5.3 eV. The nondirect transitions are due primarily to a peak at -1.9 eV in the valence-band effective density of states and a gentle peak at 6.2 eV in the conduction-band effective density of states. A deep valence band, tentatively identified as the cadmium $4d$ band, has been located at 10.3 eV below the valence-band maximum.

I. INTRODUCTION

We have used photoemission experiments to study the electronic structure of CdTe over a region extending from about 10 eV below to 10 eV above the valence-band maximum. Whereas conventional optical experiments determine only the energy differences between quantum levels, photoemission measurements determine the absolute energies of the levels involved in an electronic transition.

Recent theoretical work[1] suggests that structure in the reflectivity and other optical properties of semiconductors may be explained by "direct" electronic transitions at specific regions of the Brillouin zone and the energy gap between these levels can be determined by measuring the photon energy of strong structure in the optical data. By analyzing the photoemission data in detail we are able to determine explicitly whether or not direct transitions suffice to explain the photoemission and optical data. Although much of the structure is found to be due to direct transitions, there are a significant number of nondirect transitions. The direct transitions which we show to be present allow us to locate the absolute energies of several levels in the CdTe band structure and we compare our results with recent band calculations. The nondirect transitions allow us to locate the energies of peaks in the density of states.[2]

Cardona and Greenaway's assignments of structure in their reflectivity data[3] to specific regions of the Brillouin zone were based principally on an extrapolation of the assignments in Sn and InSb. In addition the assignments of several doublets were determined by assuming that the splittings were due to spin-orbit splitting. Since the photoemission experiment allows measurement of the absolute energies of the initial and final states for an electronic transition, it provides an independent check of these assignments. In an earlier publication[4] we examined three of these assignments in the range $5.8 \leq \hbar\omega \leq 8.0$ eV and found them to be inconsistent with the photoemission data. In the present work we discuss new assignments for this structure. Additional structure lying at higher energy is examined, and suggestions are made as to its assignment.

II. THEORY AND METHODS FOR DATA ANALYSIS

If the initial and final states for an electronic transition are the one-electron states of band theory and if Koopmans' theorem is applied, then the wave vectors of the initial and final states must be practically identical. As discussed by Spicer,[2] this selection rule causes the energy distributions of the photoemitted electrons (frequently referred to as energy distribution curves, EDC) to have features which allow us to detect the occurrence of these direct transitions. These features are summarized in Table I. The energy of the initial

TABLE I. Features of NEDC characteristic of direct and nondirect transitions.

Model	Features of NEDC
Direct transitions	Energy of initial state is a function of $\hbar\omega$; hence peaks move $\Delta(E_p) \neq \Delta(\hbar\omega)$.
	Strength determined by joint density of states; hence structure appears and disappears as $\hbar\omega$ is varied.
Nondirect transitions	Strength determined by density of states product;
	Peaks move $\Delta(E_p) = \Delta(\hbar\omega)$ (valence-band structure).
	Peaks do not move[a] (conduction-band structure).

[a] Although transport effects also result in peaks which move only slightly with photon energy, in Sec. IV we show that there is no evidence for any of these transport effects in the CdTe NEDC.

* Work supported by the National Aeronautics and Space Administration, the Advanced Research Projects Agency through the Center for Materials Research at Stanford University, and the National Science Foundation.

† Based on a dissertation submitted by J. L. Shay to Stanford University in partial fulfillment of the requirements of the Ph.D. degree.

‡ National Science Foundation predoctoral fellow.

[1] For an extensive review, see J. C. Phillips, in *Solid State Physics*, edited by F. Seitz and D. Turnbull (Academic Press Inc., New York, 1966), Vol. 18, p. 55.

[2] W. E. Spicer, Phys. Rev. 154, 385 (1967).

[3] M. Cardona and D. L. Greenaway, Phys. Rev. 131, 98 (1963).

[4] J. L. Shay, W. E. Spicer, and Frank Herman, Phys. Rev. Letters 18, 649 (1967).

state varies with photon energy, and as a result peaks in the EDC move with changes in energy unequal to the changes in photon energy. Furthermore, the strength of a transition is determined by the joint density of states, and as a result structure appears and disappears in the EDC as $\hbar\omega$ is varied.

Although ordinary one-electron band theory requires conservation of wave vector in an optical transition, the EDC from a number of materials[5–9] cannot be explained by direct transitions. These studies find that conservation of wave vector does not provide an important optical selection rule, and for many of these materials a knowledge of the density of states is sufficient to predict the experimental EDC. Conversely, a density of states (usually called the optical or effective density of states) can be obtained from the EDC. These latter electronic transitions, in which $\mathbf{k}$ conservation does not provide an important selection rule, are referred to as nondirect transitions. Features of the EDC characteristic of nondirect transitions are also listed in Table I. Since the strength of nondirect transitions is determined by the product of the valence and conduction-band densities of states, peaks in the EDC due to structure in the valence band move to higher energy with increments of energy equal to the changes in photon energy, and peaks in the EDC due to structure in the conduction band do not move as the photon energy is varied.[10] (For more details, see Ref. 2.)

Methods have been developed for determining the electronic density of states from photoemission data when the EDC result from nondirect transitions. Spicer[11] was the first to derive a valence-band optical density of states from EDC. Berglund and Spicer[5] analyzed materials in which the structure was predominantly in the valence band, and Kindig and Spicer[6] developed a detailed method for cases in which strong structure occurs in both the conduction band and the valence band. The analysis used here is due to Eden and Spicer.[12] If the nondirect model is sufficient to explain the photoemission data, then the method used here derives the same density of states as do the earlier methods. When the photoemission data is due to a mixture of direct and nondirect transitions (as is the case for CdTe), the present method explicitly separates the portions of the EDC due to direct transitions from those due to nondirect transitions. In the Appendix we discuss the details of this analysis and present a simple example of its application.

III. EXPERIMENTAL METHODS

Many of the experimental methods used in this work have been reported previously[13–15] and for this reason they are only outlined here. The experiments have been performed on CdTe single crystals cleaved in vacuum in the (110) plane. High-vacuum experiments were performed at pressures near 10^{-9} Torr using a modified version of the sample chamber and vacuum system described by Kindig and Spicer.[14] Other high-vacuum experiments used the sample chamber and vacuum systems described by Powell.[16]

The sample chamber was not continuously pumped during earlier high-vacuum experiments.[6,14] Otherwise, when the magnet used with the VacIon pump was left in place, the magnetic field distorted the EDC. For the present studies we placed a magnetic shield around the magnet. Since it was no longer necessary to remove the magnet for the duration of an experiment, the sample chamber was continuously pumped. The shield consisted of a 0.031-in. thick layer of Netic alloy within a 0.031-in.-thick layer of Conetic alloy. At the sample chamber, the field due to the magnet was reduced from about 5 G to a value much less than the earth's magnetic field.

Although it is desirable to cleave in a very good vacuum in order to study properties characteristic of the solid, we were motivated to also cleave at a poorer pressure for two reasons: (1) In these low-vacuum experiments there is no window between the light source and the cleaved crystal; hence measurements can be extended beyond the ~11.7-eV cutoff of the LiF window which seals the high-vacuum chamber. (2) The large threshold for photoemission (~6 eV) measured when the samples were cleaved in high vacuum was reduced by more than a volt when the sample was cleaved in the vacuum of the monochromator (for details see Sec. IV).

To perform a low-vacuum experiment, a low-vacuum sample chamber[15] is sealed with an O ring to the exit

[5] C. N. Berglund and W. E. Spicer, Phys. Rev. **136**, A1030 (1964); **136**, A1044 (1964).
[6] N. B. Kindig and W. E. Spicer, Solid State Commun. **2**, 13 (1964); Phys. Rev. **138**, A561 (1965).
[7] A. J. Blodgett and W. E. Spicer, Phys. Rev. Letters, **15**, 29 (1965); Phys. Rev. **146**, 390 (1966).
[8] A. J. Blodgett, W. E. Spicer, and A. Y-C. Yu, in *Optical Properties and Electronic Structure of Metals and Alloys, Proceedings of the International Colloquium, Paris, 1965* (North-Holland Publishing Company, Amsterdam, 1966), p. 246.
[9] W. E. Spicer, in *Optical Properties and Electronic Structure of Metals and Alloys, Proceedings of the International Colloquium, Paris, 1965* (North-Holland Publishing Company, Amsterdam, 1966), p. 296.
[10] A stationary peak alone is not sufficient evidence of nondirect transitions to a conduction-band density of states, since stationary peaks can also arise from electron-electron scattering (Refs. 5 and 19) or electron-phonon scattering (Ref. 20) although there is as yet no convincing experimental evidence for the latter effect. Sufficient evidence of nondirect transitions is the motion of a valence-band peak through a conduction-band peak at a photon energy corresponding to structure in the optical data as in CdS (Ref. 6) and CdSe (Ref. 24).
[11] W. E. Spicer, Phys. Rev. Letters **11**, 243 (1963).
[12] R. C. Eden and W. E. Spicer (to be published); R. C. Eden, Ph.D. dissertation, Stanford University, 1967 (unpublished); Solid State Electronics Laboratory Technical Report No. 5221–1 (unpublished).
[13] W. E. Spicer and C. N. Berglund, Rev. Sci. Instr. **35**, 1665 (1964).
[14] N. B. Kindig and W. E. Spicer, Rev. Sci. Instr. **36**, 759 (1965).
[15] J. L. Shay, Ph.D. dissertation, Stanford University, 1966 (unpublished); Solic State Electronics Laboratory Technical Report No. 5216–1 (unpublished).
[16] R. J. Powell, Ph.D. dissertation, Stanford University, 1967 (unpublished); Solid State Electronics Laboratory Technical Report No. 5220–1 (unpublished).

housing of the McPherson vacuum monochromator, model 225. Since the monochromator's oil-diffusion pump evacuates the sample chamber as well as the monochromator, a sample cleaved in the low-vacuum chamber is exposed to a base pressure of 10^{-7} Torr or a pressure of about 10^{-4} Torr when hydrogen is flowing through the arc during measurements.

A larger region of the conduction band is exposed in the low-vacuum experiments due to the reduced electron affinity. We are confident that the features of the EDC in this energy range are characteristic of CdTe for several reasons: (1) The structure in the EDC correlates well with the structure in the optical constants (see Sec. IV). (2) The optical constants were measured on samples exposed to atmospheric pressure (whereas the poorest pressure used in these photoemission experiments was 10^{-4} Torr). (3) The features of the EDC at higher energies are the same for low- and high-vacuum-cleaved samples (for example, see Fig. 17). However, the details of low-vacuum data differ somewhat from the high-vacuum data because of an increased amount of inelastic scattering in the low-vacuum-cleaved sample.

The EDC were measured using the ac method described by Spicer and Berglund.[13] The estimated uncertainty in the location of structure in the EDC is ± 0.2 eV. All measurements were performed at room temperature. The low-vacuum yield measurements used a Cs_3Sb phototube for measuring light intensity. The absolute response of the Cs_3Sb tube has been calibrated[17] against a Reeder vacuum-thermopile, and the estimated uncertainty in this calibration is $\pm 10\%$. The high-vacuum yield measurement used a sodium salicylate film for measuring relative light intensity assuming that the film's response is independent of photon energy, and the absolute yield was measured at 7.8 eV using the Cs_3Sb phototube. Since the quantum yield is the total number of photoemitted electrons per incident photon, the EDC have been normalized by requiring that the area under an EDC equals the yield at that photon energy. Energy-distribution curves that have been normalized to the yield will be called NEDC (normalized EDC).

IV. PRESENTATION OF PHOTOEMISSION DATA AND CORRELATION WITH OPTICAL DATA

In this section we present the photoemission data and examine the NEDC to determine the energies of the initial and final states leading to structure in the optical data. In Sec. V we use the density-of-states analysis (Sec. II and Appendix) to determine explicitly which of the structure in the NEDC is due to direct transitions and which is due to nondirect transitions. In Sec. VI we compare these results of the photoemission experiments with the pseudopotential band calculation by Cohen and Bergstresser[18] and with the orthogonalized-plane-wave (OPW) band calculation by Herman.[4]

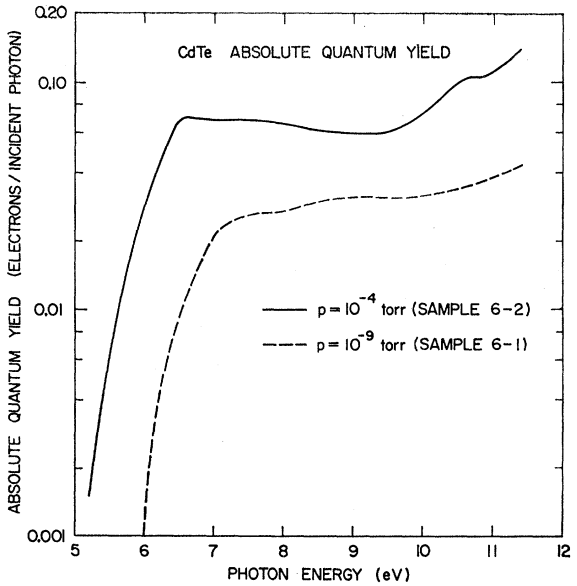

FIG. 1. Absolute quantum yield for samples of CdTe cleaved in vacuum.

A. Quantum Yield

The spectral distributions of the quantum yield for a sample of CdTe cleaved in high vacuum and for a sample cleaved in low vacuum are presented in Fig. 1. The low-vacuum experiment resulted in an electron affinity more than a volt lower than for the sample cleaved at a pressure of 10^{-9} Torr, an increase in yield at all photon energies, and a rise in yield for photon energies greater than about 9 eV. Later, using energy distributions, we show that this rise in yield is due to the escape of secondary electrons.

B. Energy Distribution Curves

1. *Low-Vacuum Experiments* (*Pressure* $= 10^{-4}$ Torr)

In Figs. 2–7 we present normalized energy-distribution curves (NEDC) for a sample cleaved at a pressure of 10^{-4} Torr. Except for $\hbar\omega = 16.8$ and 21.2 eV, all NEDC have been normalized to the yield so that the abscissa is calibrated in electrons per photon per electron volt, and electron energies are stated relative to the valence-band maximum. For a discussion of the calibration of the energy scale see Ref. 6 and 15.

The principal features of the low-vacuum NEDC are the peaks P1 and P2 and the shoulders S1 and S2. For $\hbar\omega \geq 9.2$ eV a low-energy peak appears in the NEDC and eventually dominates the other structure. The position and photon energy dependence of this station-

[17] Much of this work has been performed in our laboratory by R. Koyama.

[18] M. L. Cohen and T. K. Bergstresser, Phys. Rev. 141, 789 (1966).

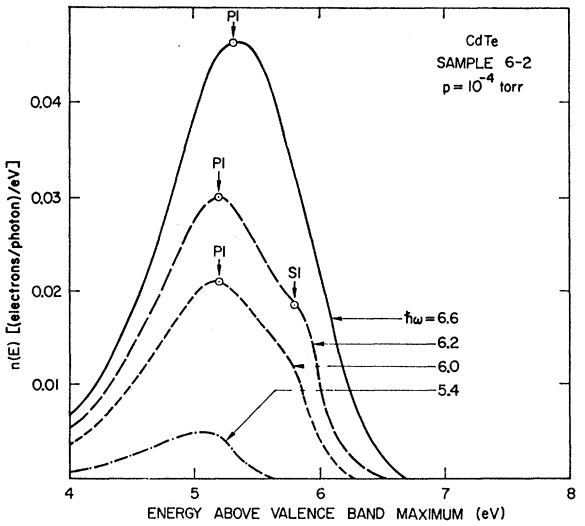

FIG. 2. Normalized energy distributions of the photoemitted electrons for the low-vacuum-cleaved sample. $5.4 \leq \hbar\omega \leq 6.6$ eV.

ary peak of low-energy electrons are characteristic of a peak due to the escape of secondary electrons produced via the pair-production mechanism.[5,19] The occurrence of this peak in the NEDC indicates that the rise in low-vacuum yield for $\hbar\omega \geq 9$ eV is due to the escape of these secondary electrons.

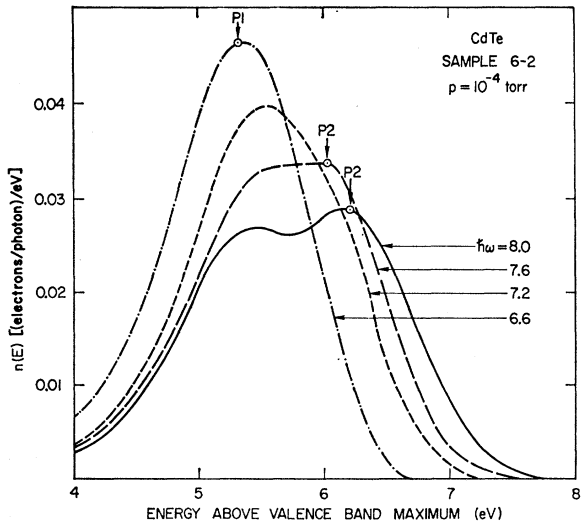

FIG. 3. Normalized energy distribution of the photoemitted electrons for the low-vacuum-cleaved sample. $6.6 \leq \hbar\omega \leq 8.0$ eV.

Before discussing the rich structure in the low-vacuum NEDC for $5.4 \leq \hbar\omega \leq 9.2$ eV, it is important to eliminate the possibility that the structure is due to transport effects. Kane[20] has recently suggested that, due to the combined effects of (1) low-group velocity at critical points and (2) phonon scattering, band structure may impress itself on photoemission through transport effects rather than through optical transition probability. As Kane points out, this will result in structure that does not move as the photon energy is varied, but is stationary in energy for $\hbar\omega$ greater than some minimum value. As can be seen from Figs. 2–7, none of the structure observed in CdTe falls into this category except for the low energy peak due to scattered electrons for $\hbar\omega > 9.2$ eV as discussed in the preceding paragraph.

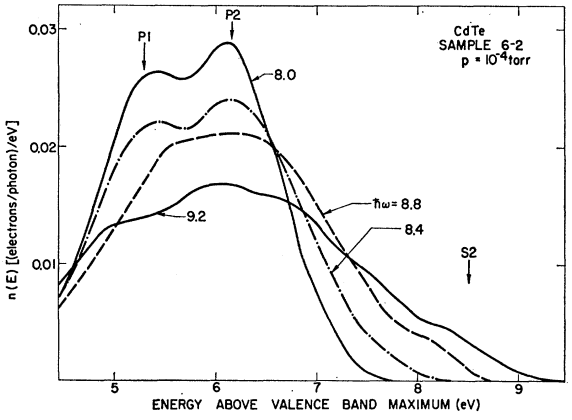

FIG. 4. Normalized energy distributions of the photoemitted electrons for the low-vacuum-cleaved sample. $8.0 \leq \hbar\omega \leq 9.2$ eV.

Any distortion of the NEDC due to these transport effects due to phonon scattering would appear not to be detectable within the limit of our resolution (±0.2 eV). Rather, peaks appear and disappear rather abruptly. Thus we can rule out the possibility that the structure to be discussed below is due to transport effects.

The peak P1 dominates the NEDC for photon energies near 6.6 eV (Figs. 2 and 3). When it has its maximum amplitude for $\hbar\omega = 6.6$ eV, P1 occurs at an

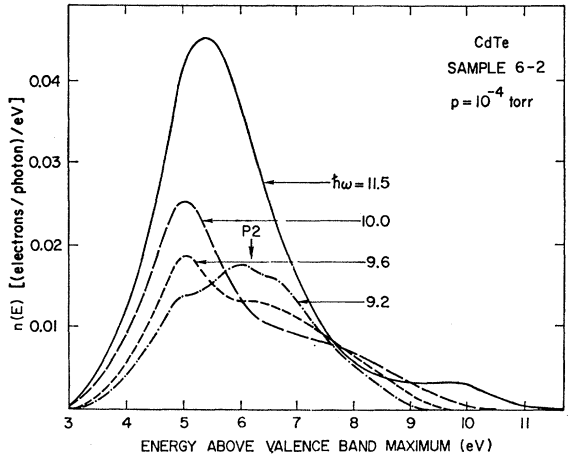

FIG. 5. Normalized energy distributions of the photoemitted electrons for the low-vacuum-cleaved sample. $9.2 \leq \hbar\omega \leq 11.5$ eV.

[19] L. Apker, E. A. Taft, and J. Dickey, J. Opt. Soc. Am. 43, 78 (1953); W. E. Spicer, J. Phys. Chem. Solids, 22, 365 (1961).

[20] E. O. Kane, in *Proceedings of the International Conference on the Physics of Semiconductors, Kyoto, 1966* [J. Phys. Soc. Japan 21, 37 (1967)].

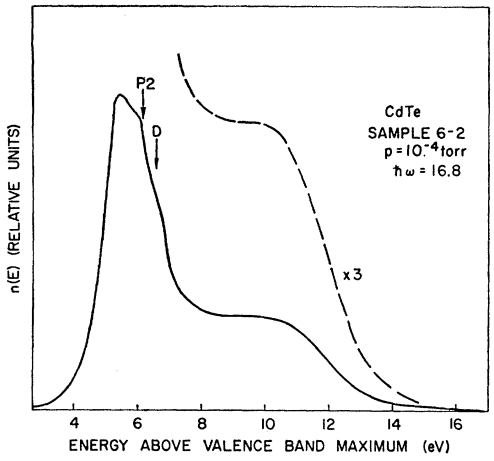

FIG. 6. Energy distribution of the photoemitted electrons for the low-vacuum-cleaved sample. $\hbar\omega = 16.8$ eV.

energy 5.3 eV above the valence-band maximum. This structure in the NEDC coincides with the peak at 6.8 eV in the reflectivity measured by Cardona and Greenaway[3] (E_1' in Fig. 8). Hence the photoemission data determine that the structure in the optical data for $\hbar\omega$ near 6.6 eV is due to transitions from valence-band states near -1.3 eV to conduction-band states near 5.3 eV.

The electrons contributing to peak P1 have not been electron-electron scattered from higher energies. For

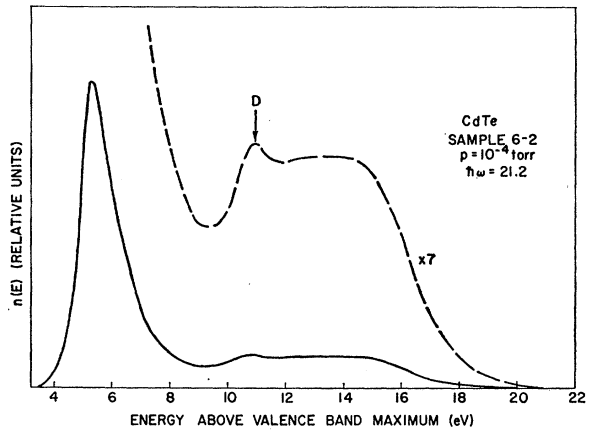

FIG. 7. Energy distribution of the photoemitted electrons for the low-vacuum-cleaved sample. $\hbar\omega = 21.2$ eV.

$\hbar\omega = 6.6$ eV there are no secondary electrons at 5.3 eV since 5.3 eV is less than a bandgap (1.6 eV) below $\hbar\omega$, and the minimum energy loss through electron-electron scattering is equal to the band gap. The abrupt disappearance of P1 for $\hbar\omega > 8.4$ eV indicates that the lower limit of the valence band has been reached at about -3.1 eV and is further evidence that a negligible fraction of this peak is due to scattered electrons. This disappearance of P1 for $\hbar\omega \gtrsim 8.4$ eV is not explained by any of Kane's[20] suggested transport effects and is convincing evidence that the structure in the CdTe NEDC is not due to transport effects.

The features of the peak P2 in the NEDC (Figs. 3 and 4) are complicated and require the density of states analysis (Sec. V) for a complete description. The qualitative features of P2 are that it is sharpest for

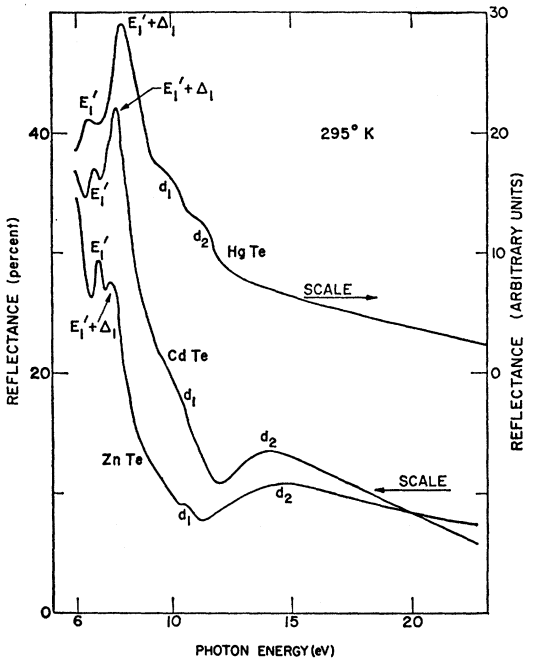

FIG. 8. Reflectivity of CdTe, ZnTe, and HgTe measured by Cardona and Greenaway (Ref. 3), $\hbar\omega > 6.0$ eV.

$\hbar\omega \approx 8.0$ eV, yet it is strongest for $\hbar\omega \approx 7.6$ eV. Corresponding to this structure in the NEDC there is a single peak at 7.6 eV in the reflectivity ($E_1'+\Delta_1$ in Fig. 8). In Sec. V we use the density of states analysis to show that the structure in the NEDC near $\hbar\omega = 8.0$ eV

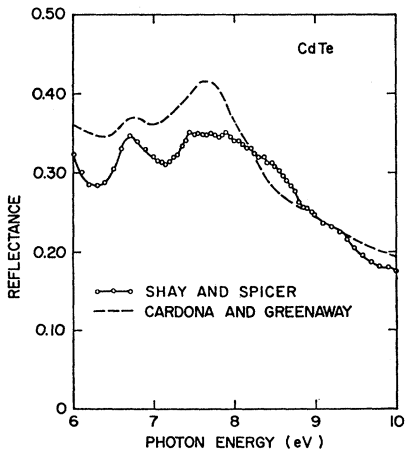

FIG. 9. Comparison of CdTe reflectivity measured by Cardona and Greenaway (Ref. 3) with the reflectivity measured by Shay and Spicer (Ref. 21).

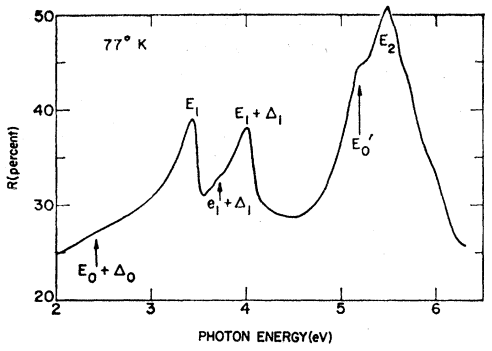

FIG. 10. Reflectivity of CdTe measured by Cardona and Greenaway (Ref. 3), $\hbar\omega<6.0$ eV.

consists of portions due to both direct and nondirect transitions. The direct transitions are strongest for a photon energy of about 7.2 eV, whereas the nondirect transitions are strongest for $\hbar\omega=8.0$ eV when a peak in the valence-band density of states near -1.8 eV is coupled to a maximum in the conduction-band density of states at 6.2 eV (P2 in Fig. 3).

This multiplicity of structure in the photoemission data suggested further study of the reflectivity in the vicinity of $\hbar\omega=8.0$ eV. The new reflectivity data[21] show much structure not observed earlier. We show in Fig. 9 the new data in the region between 6 and 10 eV and compare our results with earlier data.[3] The gross features of the two curves are similar, but the details are considerably different. We find that the relative amplitudes of the 6.8 and 7.6 eV reflectivity peaks are much different than previously reported. Of more importance to the present discussion, we find that the structure near 7.6 eV is not merely a single peak as previously found,[3] but consists of a peak at 7.5 eV and a broad shoulder near 8.0 eV. Although we would hesitate to refer to this multiplicity at 7.6 eV as a "doublet," it is clear that it arises from two distinct

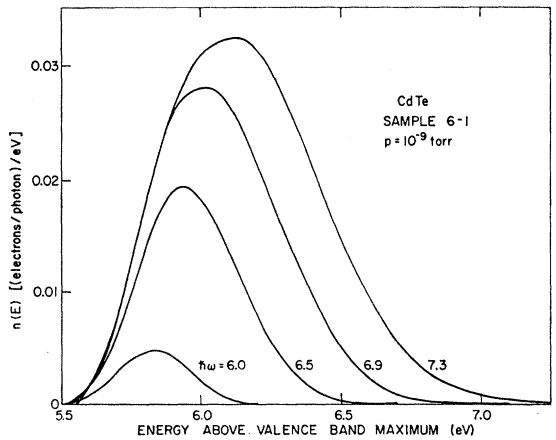

FIG. 11. Normalized energy distributions of the photoemitted electrons for the high-vacuum-cleaved sample. $6.0<\hbar\omega<7.3$ eV.

[21] J. L. Shay and W. E. Spicer (to be published).

optical transitions. In Sec. VI we suggest a possible location in the Brillouin zone for the direct transitions near $\hbar\omega\approx7.2$ eV.

For $\hbar\omega>5.8$ eV, the shoulder $S1$ appears in the NEDC (Fig. 2). Since S1 appears near the maximum energy,

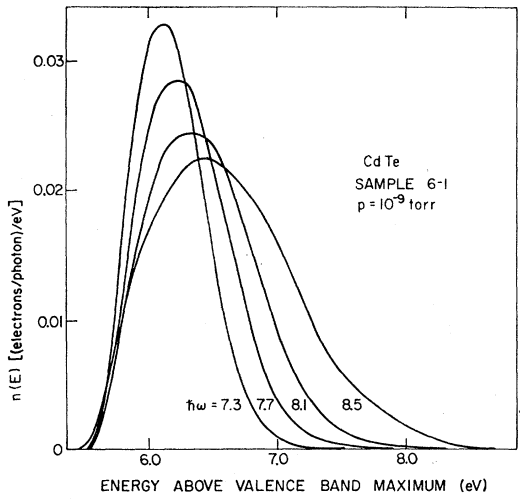

FIG. 12. Normalized energy distributions of the photoemitted electrons for the high-vacuum-cleaved sample. $7.3\leq\hbar\omega\leq8.5$ eV.

it is due to transitions from initial states near the valence-band maximum (i.e., near Γ_{15v}) to conduction-band states near 5.8 eV. Corresponding to S1 there is a slight shoulder near 5.8 eV in the reflectivity (Fig. 10). For $\hbar\omega>8.7$ eV another shoulder S2 appears in the

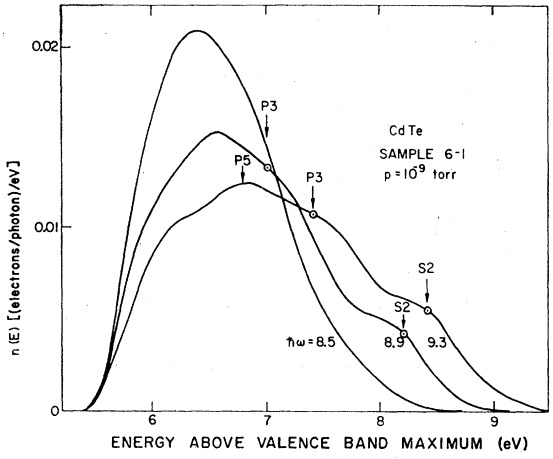

FIG. 13. Normalized energy distributions of the photoemitted electrons for the high-vacuum-cleaved sample. $8.5\leq\hbar\omega\leq9.3$ eV.

NEDC. Like S1, S2 also appears near the maximum energy, and hence is due to transitions from initial states near the valence-band maximum to conduction-band states near 8.7 eV. The edge of the broad optical structure labelled d_1 in Fig. 8 begins near 8.7 eV corresponding to the appearance of S2 in the NEDC.

In Figs. 6 and 7 we present EDC for $\hbar\omega=16.8$ and 21.2 eV. Most of the photoemitted electrons have been inelastically scattered from higher energies. For $\hbar\omega=21.2$ eV the peak of electrons labelled D at 10.9 eV in

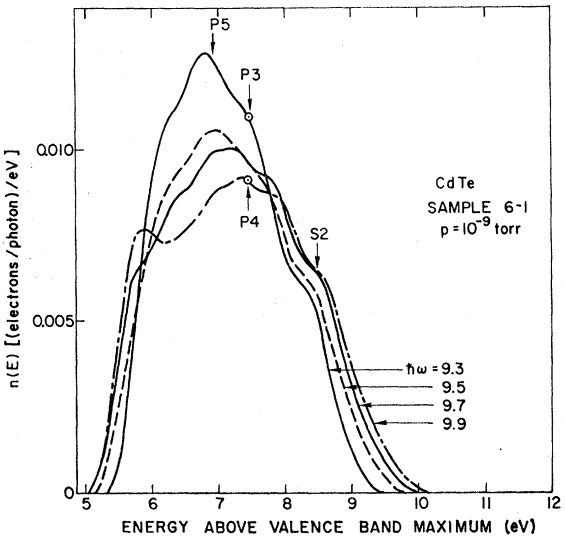

FIG. 14. Normalized energy distributions of the photoemitted electrons for the high-vacuum-cleaved sample. $9.3\leq\hbar\omega\leq9.9$ eV.

Fig. 7 is believed to be due to transitions from a high density of states at -10.3 eV in the valence band. We suggest that these valence-band states are derived from

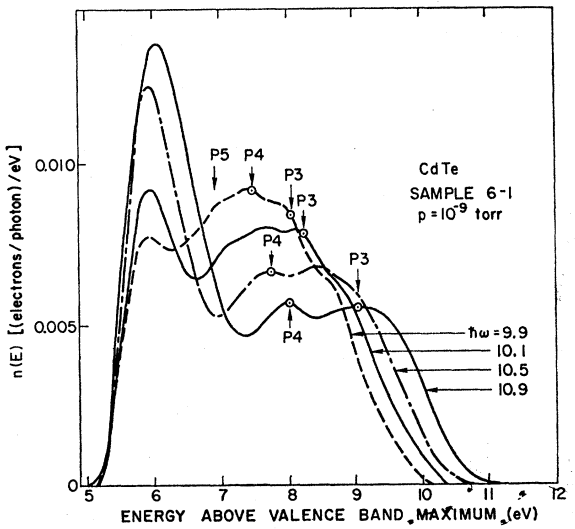

FIG. 15. Normalized energy distributions of the photoemitted electrons for the high-vacuum-cleaved sample. $9.9\leq\hbar\omega\leq10.9$ eV.

cadmium $4d$ states since on the cadmium ion the $4d$ states lie about 9 eV below the $5s$ states.[22] We cannot

[22] C. E. Moore, *Atomic Energy Levels*, Natl. Bur. Std. Cir. No. 467 (U. S. Government Printing Office, Washington, D. C., 1949).

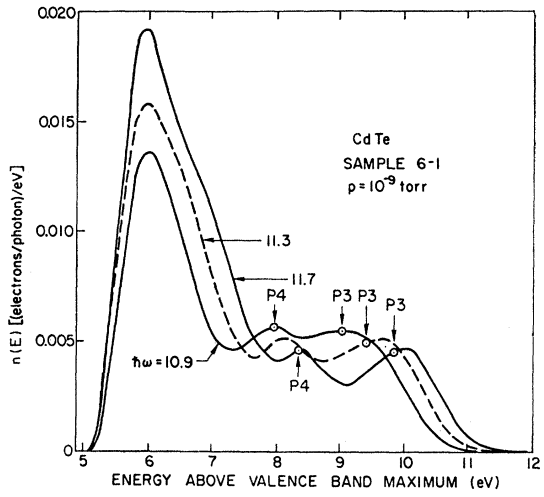

FIG. 16. Normalized energy distributions of the photoemitted electrons for the high-vacuum-cleaved sample. $10.9\leq\hbar\omega\leq11.7$ eV.

rule out the possibility that peak D is due to the valence band splitoff by about 10 eV from the others. However, the density of states for this valence band is only 2 electrons per molecule whereas there are ten d electrons per molecule. In the future, the origin of peak D may be established from optical data by applying the sum rule which relates total absorption to the number of electrons contributed by each molecule.

It is not possible to follow the motion of peak D over a wide range of photon energy to confirm its origin in the valence band; however, if the peak were due to conduction band structure near 10.9 eV, we would expect to see a peak at 10.9 eV for $\hbar\omega=16.8$ eV. No such peak is seen in Fig. 6. On the other hand, if the peak at 10.9 eV for $\hbar\omega=21.2$ eV is in fact due to excitation from valence-band states near -10.3 eV, then for $\hbar\omega=16.8$ eV this peak of electrons should be seen at 6.5 eV. The structure labelled D at 6.5 eV in Fig. 6 is believed to be due to these transitions. It is not clear

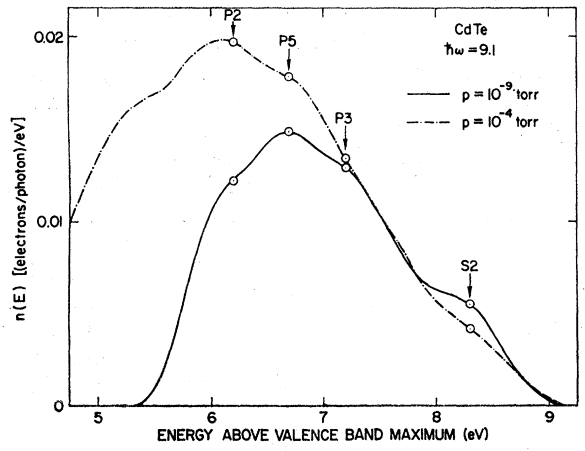

FIG. 17. Comparison of normalized energy distributions from high- and low-vacuum-cleaved samples of CdTe, $\hbar\omega=9.1$ eV.

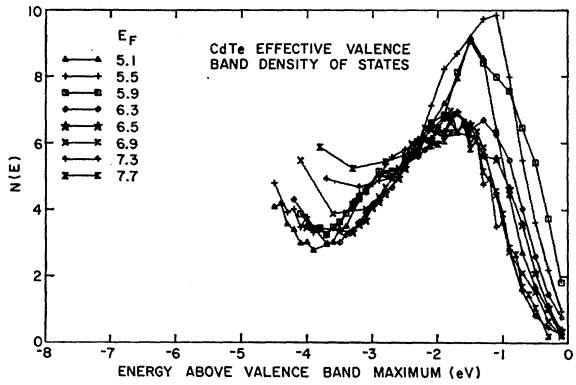

FIG. 18. CdTe effective valence-band density of states determined by density-of-states analysis of low-vacuum photoemission data (sample 6–2). E_f is the energy of the conduction-band state used to derive the effective valence-band density of states. These curves do not superimpose due to direct transitions.

whether the structure labeled P2 at 6.2 eV in Fig. 6 is due to excitation from the d band to the conduction-band states previously located at 6.2 eV or due to preferential scattering to this high density of states. We prefer the former suggestion since P2 is not seen in Fig. 7 for $\hbar\omega=21.2$ eV where the peak of scattered electrons is strongest. The d_2 reflectivity peak at 14 eV in Fig. 8 has been interpreted as resulting from transitions from the cadmium $4d$ band. Since the photoemission data have located these valence-band states at -10.3 eV, structure in the optical data near 14 eV is due to transitions to conduction-band states near 3.7 eV.

2. *High-Vacuum Experiments* (Pressure = 10^{-9} Torr)

In Figs. 11–16 we present NEDC for a sample of CdTe cleaved at a pressure of 10^{-9} Torr. The striking difference between these curves and the energy distributions for the sample cleaved in the monochromator vacuum (Figs. 2–7) is that the electron affinity is more than a volt larger for this high-vacuum cleavage.[23,24] Because of the increased electron affinity, some of the structure seen in the low-vacuum NEDC is not observed here. In addition, the number of secondary electrons appearing in the energy distributions is much smaller than for the low-vacuum-cleaved sample and new structure is resolved in the high-vacuum data.

We compare in Fig. 17 NEDC from high- and low-vacuum experiments for a photon energy of 9.1 eV. The superposition of these curves at high energies is somewhat surprising since the threshold functions (surface transmission probabilities) will differ because of the difference in electron affinity. Furthermore, the absolute yield for the high-vacuum experiment may be somewhat in error since it depends upon the uniform response assumed for the sodium salicylate film (see Sec III). The essential point of Fig. 17 is that there is a one-to-one correspondence between the structure in the high-vacuum data and in the low-vacuum data. The principal effect of the poorer vacuum is a lowering of the electron affinity.

The principal features of the high-vacuum NEDC are the peaks P3, P4, and P5 and the shoulder S2. The peaks P3 and P5 as well as the shoulder S2 were also observed in the low-vacuum data (see in particular Fig. 17). It is apparent in Figs. 14–16 that this structure is due to transitions from a valence band that is 3.5 to 4.0 eV wide. The decrease in amplitude of the peaks as they move to higher energies indicates that the fraction of the electrons lost due to inelastic scattering increases rapidly with increasing electron energy. For $\hbar\omega\geq 9.7$ eV a large low energy peak appears in the NEDC. As in the low-vacuum data, this stationary peak of low-energy electrons is characteristic of a peak due to the escape of secondary electrons.[5,19] The structure P2 in the low-vacuum NEDC (Figs. 3–5) is not resolved as a peak in the high-vacuum data (Figs. 11–16) due to the increased electron affinity, although it accounts for the maximum in the NEDC for $\hbar\omega\approx 7.3$ eV (Fig. 12) and the low-energy shoulder for $8.5\leq\hbar\omega\leq 9.7$ eV.

For $\hbar\omega\geq 8.7$ eV the shoulder S2 appears in the NEDC (Figs. 13–15). As in the low-vacuum data, S2 appears near the maximum energy indicating that it is due to transitions from initial states near the valence-band maximum to conduction-band states near 8.7 eV. When S2 first appears for $\hbar\omega$ near 8.7 eV, the largest fraction of these electrons are photoemitted near 8.2 eV, and hence they have initial states at -0.5 eV. This reflects the fact that the density of states vanishes at the top of the valence band, and the largest transition probability occurs for initial states slightly below the top of the valence band. S2 moves to higher energies only slightly for increasing photon energy moving 0.5 eV while the photon energy is increased by 1.4 eV to 10.1 eV. For $\hbar\omega>$ 10.1 eV, S2 disappears from the NEDC.

A peak P5 appears at 6.9 eV for $8.5\leq\hbar\omega\leq 10.1$ eV (Figs. 13–15). The fact that P5 is always seen at 6.9 eV indicates that it is due to nondirect transitions to a peak at 6.9 eV in the conduction band density of states. The disappearance of P5 for $\hbar\omega\gtrsim 10.1$ eV reflects a valence-band width of 3.5–4.0 eV and indicates that P5 is not due to electrons scattered from higher energies. The peaks P3 and P4 both seem to originate from peak P5 near 6.9 eV. For $\hbar\omega\gtrsim 8.9$ eV (Figs. 13–16) P3 splits from P5 and moves to higher energies with its location approximately given by

$$E_{P3}=\hbar\omega-1.9\text{ eV}. \quad (1)$$

The motion of P3 in accordance with Eq. (1) indicates that it is due to nondirect transitions from a peak at -1.9 eV in the valence-band density of states, and that conservation of wave vector is not an important selection rule for the transitions associated with P3 (see

[23] A reduced electron affinity due to the 10^{-4} vacuum has also been observed in CdS (Refs. 6, 15, and 24) and in CdSe (Refs. 15 and 24).

[24] J. L. Shay and W. E. Spicer (to be published).

Table I). In the low-vacuum experiment this valence-band peak near -1.9 eV is coupled to a peak at 6.2 eV in the conduction-band density of states and accounts for peak P2 in Figs. 3 and 4 for $\hbar\omega=8.0$ eV.

For $\hbar\omega \gtrsim 9.3$ eV the peak P4 splits from P5 and moves to higher energies with its location approximately given by

$$E_{P4}=0.5\ \hbar\omega+2.5\ \text{eV}. \quad (2)$$

The motion of P4 in accordance with Eq. (2) indicates that P4 is due to direct transitions (see Table I). Hence, P4 trails P3, with their separation increasing as the photon energy is increased. It is apparent in Fig. 16 that P4 is moving much more slowly than P3 since the valley between them is deepening as the photon energy is increased; P3 is "walking away" from P4. This is a striking example of the simultaneous presence of direct and nondirect transition in the same sample for the same photon energies.

The structure observed in the photoemission data is summarized in Table IV. This table also contains information discussed in Secs. V and VI which follow.

V. DENSITY OF STATES ANALYSIS OF PHOTOEMISSION DATA

In this section we determine explicitly which structure in the NEDC is due to direct transitions and which structure is due to nondirect transitions. When direct transitions occur in the NEDC, this analysis determines many details about the band structure and these will be discussed in Sec. VI.

A. Low-Vacuum Data

In Figs. 18 and 19 we present the valence-band and conduction-band effective densities of states derived from the low-vacuum data. The values of the density of states used to derive these results are shown in Table II, and the details of this analysis are discussed in the Appendix. In Figs. 18 and 19 and Table II, E_f indicates the energy of the final state used to derive the effective valence-band density of states, and E_i indicates the energy of the initial state used to derive the effective conduction-band density of states. Recall that if the valence-band densities of states seen by various final energies superimpose and if the conduction-band densities of states seen by various initial energies

TABLE II. Scale factors for density-of-states analysis of low-vacuum photoemission data for CdTe.

E_i	$N_v(E_i)$	E_f	$N_c^{\text{eff}}(E_f)$
-0.7	2.32	5.1	2.94
-0.9	3.20	5.5	2.91
-1.3	5.38	5.9	2.60
-1.7	6.82	6.3	2.50
-2.1	6.14	6.5	2.16
-2.5	5.61	6.9	1.50
-2.9	4.82	7.3	1.10
		7.7	0.83

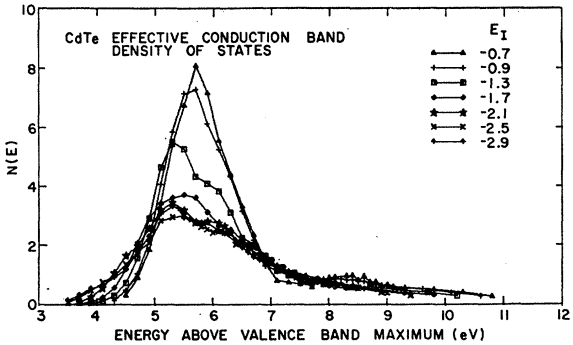

FIG. 19. CdTe effective conduction-band density of states determined by density-of-states analysis of low-vacuum photoemission data (sample 6-2). E_i is the energy of the initial state used to derive the effective conduction-band density of states. These curves do not superimpose due to direct transitions.

superimpose, then one must conclude that the nondirect model is sufficient to explain the photoemission from CdTe. In some regions of Figs. 18 and 19, two curves differ by as much as a factor of 3. This lack of superposition is due to direct transitions, and the ratio of the amplitudes of two curves indicates the strength of these direct transitions.

In those regions of Figs. 18 and 19 where the curves superimpose, the corresponding features of the NEDC are due to nondirect transitions. We see that there is a nondirect "background" in the NEDC due to a peak in the valence-band effective density of states at about -1.9 eV and gentle peaks in the conduction-band effective density of states near 5.3 and 6.2 eV. The decrease in the effective conduction-band density of states with increasing energy probably indicates that the fraction of electrons lost due to inelastic scattering increases with electron energy. The apparent rise in the effective valence-band density of states for $E \lesssim -3.6$ eV corresponds to the large peak of inelastically scattered electrons appearing in the NEDC for $\hbar\omega \gtrsim 9.2$ eV. In Fig. 20 we have sketched our estimate of the CdTe effective density of states based on the nondirect contributions to the NEDC.

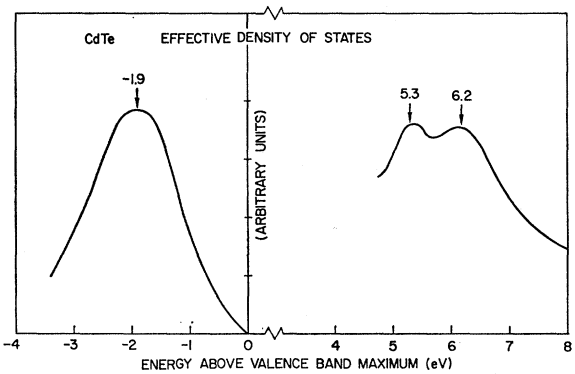

FIG. 20. CdTe effective density of states estimated from nondirect transitions observed in the energy distributions.

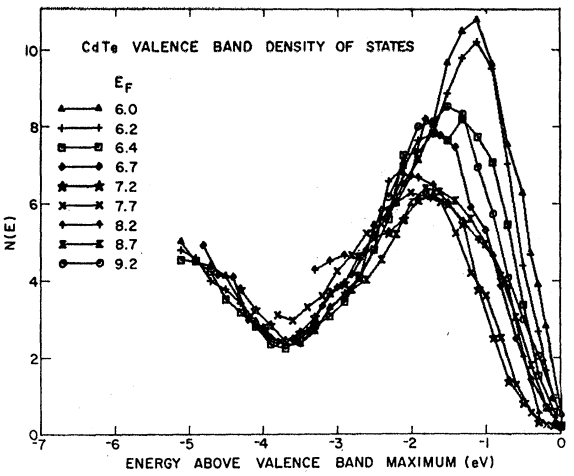

FIG. 21. CdTe effective valence-band density of states determined by density-of-states analysis of high-vacuum photoemission data (sample 6–1). E_f is the energy of the conduction-band state used to derive the effective valence-band density of states. These curves do not superimpose due to direct transitions.

We now discuss the direct transitions which this analysis shows to be present in the NEDC. In Fig. 18 the curves for $E_f=5.1$ and 5.5 eV indicate that there are numerous direct transitions to these final states from initial states near -1.3 eV. The corresponding feature of the NEDC is the peak P1 which reached a maximum amplitude for $\hbar\omega=6.6$ eV when it coupled valence-band states near -1.3 eV to conduction-band states near 5.3 eV (Figs. 2 and 3). This structure in the photoemission data correlated well with the E_1' peak at 6.8 eV in the reflectivity (Fig. 8). In Fig. 19 we see that the number of electrons excited to the conduction-band peak at 5.3 eV from initial states near -1.3 eV is about twice as much as predicted by the nondirect model. Hence we have explicitly shown that the structure P1 which appears abruptly in the NEDC for $\hbar\omega=6.6$ eV and disappears shortly thereafter (Figs. 2 and 3) is due to direct transitions.

It can be seen in Fig. 18 that the strongest direct transitions from valence-band states close to the top of the valence band are to conduction-band states near $E_f=5.9$ eV. The corresponding feature of the NEDC is the shoulder S1 (Fig. 2) which appears for $\hbar\omega\geq 5.8$ eV. We showed in Sec. IV that S1 corresponded to the slight shoulder near 5.8 eV in the reflectivity. It is apparent in Fig. 18 that the weakness of this structure is due to the small density of states close to the top of the valence band, and the strength that S1 does have is almost entirely due to direct transitions.

The peak P2 in the NEDC which remains at 6.2 eV for $\hbar\omega\geq 8.0$ eV (Figs. 3 and 4) is due to nondirect transitions to a gentle peak at 6.2 eV in the conduction-band density of states. This is obvious from Fig. 19, since all valence-band states below about -1.7 eV see approximately the same effective conduction-band density of states having a slight peak at 6.2 eV. However, for $6.6\lesssim\hbar\omega\lesssim 8.0$ eV the structure P2 in the NEDC (Figs. 2 and 3) consists of portions due to both direct and nondirect transitions. The direct transitions can be seen in Fig. 18 where final states between 5.9 and 6.5 eV show large numbers of direct transitions for valence-band states within about 1.3 eV of the top of the valence band. The nondirect transitions to the conduction-band peak at 6.2 eV are strongest for $\hbar\omega=8.0$ eV when the peak in the valence-band density of states at -1.9 eV is coupled to these final states (Figs. 2 and 3). For $\hbar\omega>8$ eV, nondirect transitions from the peak in the valence-band result in peak P3 which moves to higher energies in accordance with Eq. (1) (Figs. 13–17).

The shoulder S2 appears in the NEDC for $\hbar\omega\geq 8.7$ eV when initial states near the top of the valence band are coupled to final states near 8.7 eV. This structure is not seen in Fig. 18 because we have only included final states below 7.7 eV. For higher-lying final states the contributions due to scattering become excessive. In Fig. 19 the effective conduction-band densities of states seen by $E_i=-0.7$ and -0.9 eV peak near 8.5 eV corresponding to the appearance of S2 in the NEDC. The structure S2 is considerably sharper in the high-vacuum data (see Fig. 17).

B. High-Vacuum Data

In Figs. 21 and 22 we present the valence-band and conduction-band effective densities of states derived from the high-vacuum data. The values of the density of states used to derive these results are shown in Table III, and the details of this analysis are discussed in the Appendix.

In those regions of Figs. 21 and 22 where the curves superimpose, the corresponding features of the NEDC are due to nondirect transitions. As in the low-vacuum data (Figs. 18 and 19), we see that there is a nondirect "background" in the NEDC due to a peak in the valence-band density of states at about -1.9 eV and a

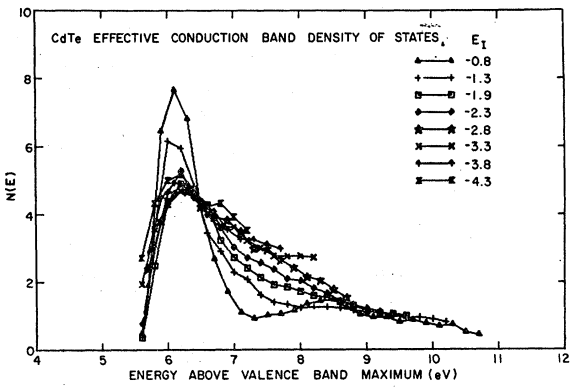

FIG. 22. CdTe effective conduction-band density of states determined by density-of-states analysis of high-vacuum photoemission data (sample 6–1). E_i is the energy of the initial state used to derive the effective conduction-band density of states. These curves due not superimpose due to direct transitions.

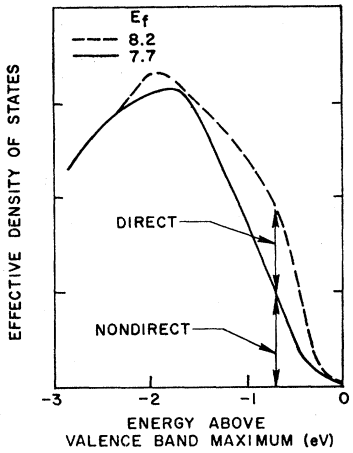

FIG. 23. Selected curves from Fig. 21 showing explicit separation of direct and nondirect transitions.

peak in the conduction-band density of states near 6.2 eV. The lower portion of this peak is distorted due to rapidly rising threshold function. The peak in the valence band explains the peak P3 which appeared in the NEDC (Figs. 13–17) and moved to higher energies in accordance with Eq. (1). In Sec. IV we showed qualitatively that this motion in accordance with Eq. (1) is characteristic of nondirect transitions, and now we have explicitly shown that the peak P3 is due to nondirect transitions from a peak at -1.9 eV in the valence-band density of states. The decrease in the effective conduction-band density of states (Fig. 22) with increasing energy suggests that the fraction of electrons lost due to inelastic scattering increases with electron energy as would be expected. We see from Fig. 21 that the valence band is about 3.7 eV wide. The apparent rise in the effective valence-band density of states for $E \leq -3.7$ eV corresponds to the appearance of secondary electrons in the NEDC.

We now discuss the direct transitions which this analysis shows to be present in the NEDC. Because of the larger electron affinity for the high-vacuum-cleaved sample, we observe only a portion of the direct transitions contributing to P2, in the low-vacuum experiment. However, as in the low-vacuum data (Fig. 18), we see in Fig. 21 that final states between about $E_f = 6.0$ and 6.7 eV show direct transitions for valence-band states within about 1.3 eV of the top of the valence band.

We now show that the shoulder S2 which appears in the NEDC for $8.7 \leq \hbar\omega \leq 10.1$ eV is due to direct transitions. This case is a good example of the power of the density of states analysis. Although the shoulder S2 accounts for only a small fraction of the NEDC, it shows up as a large effect in this analysis. In Fig. 23 we show portions of the effective valence-band densities of states seen by conduction-band energies of 7.7 and 8.2 eV. Conduction-band states at 8.2 eV are coupled by both direct and nondirect transitions to initial states within about 1.5 eV of the valence-band maximum. The total number of transitions is small because the density of states is small, but it is clear that at least half of the electrons excited to conduction-band states at 8.2 eV from initial states near -0.7 eV result from direct transitions.

We showed in Sec. IV B that P4 (Figs. 14–16) is due to direct transitions since it moves in accordance with Eq. (2). This structure is more easily seen in the NEDC than in the density of states analysis since a larger fraction of the electrons at higher energies in the NEDC are inelastically scattered before escaping. Nonetheless, the direct transitions causing P4 are also observed here. In Fig. 21 we see that there are direct transitions to final states near $E_f = 8.2$ eV from initial states near -3.0 eV.

The variations of the effective conduction-band densities of states (Fig. 22) for $7.0 \leq E \leq 8.0$ eV show that states close to the top of the valence band are weakly coupled to these final states. This variation was also observed in the low-vacuum data (Fig. 19), and accounts for the paucity of high-energy electrons in the NEDC for $\hbar\omega \approx 8.0$ eV (Figs. 3 and 12).

In summary, we have analyzed the photoemission energy distribution curves to determine explicitly whether structure is due to direct or nondirect transitions. Structure due to nondirect transitions has allowed us to determine features of the effective density of states (Fig. 20). In the following section we use the direct transitions to obtain features of the electronic band structure of CdTe.

VI. THE BAND STRUCTURE OF CdTe

In this section we assign some of the direct transitions observed in the photoemission data to specific regions of the Brillouin zone. We first show that several earlier assignments of structure in the optical data are inconsistent with the photoemission data.[4] We then make use of the photoemission data to suggest possible new assignments for the optical and photoemission structure.

Since the photoemission data will be used to determine features of the band structure, it is important that the reader understand the spirit in which this is done. Although it is usual to associate structure in optical data with symmetry points in the band structure, it is

TABLE III. Scale factors for density-of-states analysis of high-vacuum photoemission data for CdTe.

E_i	$N_v(E_i)$	E_f	$N_c^{\text{eff}}(E_f)$
-0.8	5.3	6.0	4.68
-1.3	7.8	6.2	4.86
-1.9	7.4	6.4	4.73
-2.4	5.7	6.7	3.78
-2.8	3.9	7.2	3.02
-3.3	2.8	7.7	2.27
-3.8	2.3	8.2	1.83
-4.3	3.15	8.7	1.63
		9.2	1.35

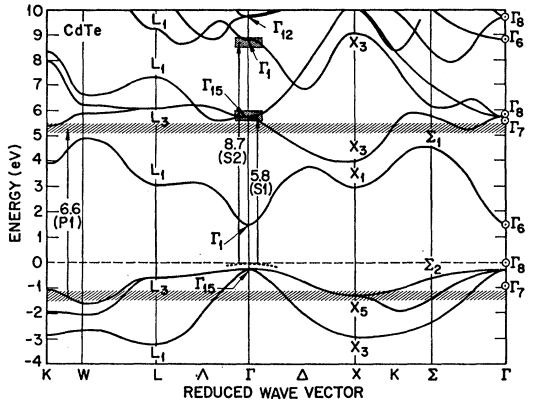

FIG. 24. Herman's OPW band structure for CdTe (Ref. 4). Cross-hatching indicates initial and final states for direct transitions located by photoemission data.

clear from recent work such as that by Kane[25] that a large region of **k** space is necessary to produce strong peaks in optical data. As a result, the energy gap at the symmetry point may not exactly equal the most probable energy for the optical transition. The photoemission data determine the final energy to which the optical transition is most probable. Although the symmetry point of the band structure may not exactly equal this energy, in the interpretation of data in this article, we will follow the usual practice of relating optical and photoemission peaks to symmetry points of the band structure. However, it must be remembered that since a large volume in **k** space is necessary for a strong direct optical transition, the optical and photoemission peaks may correspond to regions of **k** space which lie somewhat away from the symmetry points with which they are associated.

We have shown in Sec. IV that the photoemission peaks P1 and P2 (Figs. 2–4) are associated with the optical peaks at 6.8 and 7.6 eV (Fig. 8). Previously this structure in the optical data has been assigned[3,18,26] to transitions from the spin-orbit-split valence band L_{3v} to the conduction band L_{3c}. This assignment required the *final* energies to be the same for both optical peaks. From Figs. 2–4 and the discussion in Sec. IV it is clear that this is not the case, since the final state for the 6.8 eV optical peak lies at 5.3 eV and that for the 7.6 eV optical peak lies at about 6.2 eV. Thus the assignment of the two optical peaks to transitions to the same final state can be discarded at once.

The systematics of the optical data for the series ZnTe, CdTe, and HgTe also argue against the previous assignment. Theoretically, it is expected[27] that the spin-orbit splitting of the valence band should be approximately the same for the series ZnTe, CdTe, and HgTe. Experimental confirmation[3] is found for this in the splitting of the E_1 reflectivity peaks which are assigned to $L_{3v} \rightarrow L_1$ transitions: 0.56 eV (ZnTe), 0.56 eV (CdTe), and 0.62 eV (HgTe). However, for the transitions assigned to $L_{3v} \rightarrow L_{3c}$ (E_1' peaks), the splittings are quite different: 0.59 eV (ZnTe), 0.88 eV (CdTe), and 1.25 eV (HgTe). Cardona and Greenaway's data also show that the shapes and relative strengths of the E_1' peaks vary considerably among these compounds whereas this is not the case for the E_1 peaks. This suggests that the splitting of the E_1' peaks is not due to spin-orbit splitting of the valence band.

It might be suggested that the 6.8 and 7.6 eV reflectivity peaks are due to transitions to a spin-orbit-split conduction band L_{3c}. There are three arguments which indicate that this is not the case; two of these are based on the known spin-orbit splitting of the valence band L_{3v} (0.6 eV).

1. A spin-orbit-split L_{3c} would produce four optical peaks rather than the two observed.

2. The valence-band splitting would cause additional structure near both P1 and P2 in the NEDC, but none is observed.

3. Certain theoretical calculations[27,28] indicate that conduction-band spin-orbit splittings are much less than valence-band splittings of 0.6 eV, whereas the observed final-state energies for the 6.8 and 7.6 reflectivity peaks in CdTe differ by 0.9 eV.

Having shown that the 6.8 and 7.6 eV optical peaks are not due to spin-orbit-split $L_{3v} \rightarrow L_{3c}$ transitions, we look to other regions of the zone for the origins of these peaks. The initial and final states for three of the direct transitions which we observe in the photoemission data are sketched onto Herman's[4] calculated band structure in Fig. 24. We compare Herman's[4] band structure with that of Cohen and Bergstresser[18] in Fig. 25. Since we have demonstrated in Sec. V that P1 is due to direct transitions, if these band calculations are correct, they must provide a location for this structure. Although there are valence-band states at X at the energy of the initial states for P1, there are no X conduction-band states near the final states for P1. Similarly, these calculations do not permit P1 to be near either L or Γ. Herman[4] has also calculated the bands along the zone edge from W to K. These bands (Fig. 24) provide high densities of states in the valence and conduction bands corresponding to the initial and final states for P1 at a photon energy of 6.6 eV. Hence the structure P1 in the NEDC corresponding to the E_1' reflectivity peak at 6.8 eV is most likely due to direct transitions near the zone edge from W to K.

In Sec. V we demonstrated that for $\hbar\omega \approx 8.0$ eV the structure P2 in the NEDC is due to nondirect transitions from a peak near -1.8 eV in the valence-band density of states to a peak at 6.2 eV in the conduction-band density of states. Figure 24 suggests that these conduction band states lie near L_3 and the valence-band states lie near the zone edge. For photon energies above

[25] E. O. Kane, Phys. Rev. 146, 558 (1966).
[26] H. Ehrenreich, H. R. Philipp, and J. C. Phillips, Phys. Rev. Letters, 8, 59 (1962).
[27] F. Herman, C. Kuglin, K. Cuff, and R. Kortum, Phys. Rev. Letters, 11, 541 (1963).
[28] J. C. Phillips and L. Liu, Phys. Rev. Letters 8, 94 (1962).

8.0 eV P2 remains at 6.2 eV (Fig. 4) because of nondirect transitions to the peak in the conduction-band density of states, and a peak P3 (Figs. 13–16) due to nondirect transitions from the peak at −1.9 eV in the valence-band density of states moves to higher energies in accordance with Eq. (1). At lower photon energies (~7.2 eV) some of P2 is due to direct transitions to final states near 6.2 eV (Sec. V). Before discussing the origin of these direct transitions, let us discuss the shoulders S1 and S2 (Figs. 2, 4, and 13–15).

The abrupt manner in which both S1 and S2 appear in the NEDC is characteristic of direct transitions (Sec. II). In fact we have shown explicitly in Sec. V that these shoulders are due to direct transitions. Since the shoulders appear near the maximum energy, they can only be due to transitions from states near the valence-band maximum Γ_{15v}. In this article Γ_{15v} refers to the uppermost (Γ_8) of the spin-orbit-split levels Γ_{15v}. Thus we assign S1 to $\Gamma_{15v} \rightarrow \Gamma_{15c}$ transitions. Since S1 appears for $\hbar\omega$ greater than 5.8 eV, we locate Γ_{15c} at 5.8 eV. Cardona and Greenaway[3] have assigned the E_0' reflectivity shoulder (Fig. 10) at 5.2 eV to $\Gamma_{15v} \rightarrow \Gamma_{15c}$ transitions. This assignment is not consistent with the photoemission data, since transitions to Γ_{15c} only occur for $\hbar\omega > 5.8$ eV. We suggest instead that the slight shoulder at 5.8 eV in the reflectivity data is due to $\Gamma_{15v} \rightarrow \Gamma_{15c}$ transitions. S2 appears abruptly for $\hbar\omega > 8.7$ eV placing the third Γ conduction band (probably Γ_1) near 8.7 eV. Corresponding to S2, the edge of the broad optical structure labelled d_1 by Cardona and Greenaway[3] appears at about 8.7 eV. Herman's band calculation (Fig. 24) places Γ_1 at 8.8 eV in good agreement with our value. For $\hbar\omega > 8.7$ eV S2 moves slightly to higher energies until $\hbar\omega \approx 10.1$ eV. For $\hbar\omega \gtrsim 10.1$ eV S2 disappears from the NEDC indicating the termination of the bands which cause S2. Herman's band structure (Fig. 24) suggests that S2 is in part due to states in the Λ direction. In that case S2 disappears abruptly since the joint density of states decreases rapidly off the Λ axis.

Having shown that S1 is due to the direct transition $\Gamma_{15v} \rightarrow \Gamma_{15c}$, a possible origin of the direct transitions

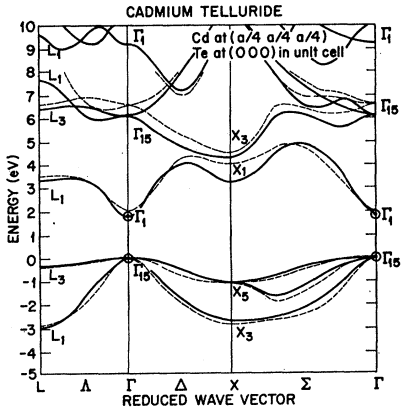

FIG. 25. Comparison of Herman's (Ref. 4) OPW band structure (solid curve) and Cohen and Bergstresser's (Ref. 18) pseudopotential band structure (dashed curve) for CdTe.

contributing to P2 becomes apparent. For $\hbar\omega > 5.8$ eV the transitions causing S1 for $\hbar\omega = 5.8$ eV move away from Γ in the general direction of L. These direct transitions do not lead to a peak in the NEDC because P1 is a much stronger transition, but they do lead to the large number of electrons excited to within 1 eV of the highest energy for $\hbar\omega$ near 7.2 eV (Fig. 3). These direct transitions were clearly seen in the density of states analysis presented in Sec. V. For $\hbar\omega \gtrsim 7.6$ eV these direct transitions drop out of the NEDC and a well defined peak P2 is observed due to the nondirect transitions to the conduction-band density of states peak at 6.2 eV from the peak at near −1.9 eV in the valence-band density of states. This peak in the valence-band density of states produces the peak P3 for $\hbar\omega \gtrsim 8.0$ eV (Figs. 13–17).

In Sec. IV we pointed out that P3 was "walking away" from P4 (Figs. 14–16) because the energy of the initial states for P4 decreased with increasing $\hbar\omega$ (direct transitions) whereas the energy of the initial states for P3 did not change with increasing $\hbar\omega$ (nondirect transitions). It is apparent from Fig. 24 that the initial

TABLE IV. Summary of CdTe photoemission data.

$\hbar\omega$	Label	Energy[a] of final state	Energy[a] of initial state	Nature of transition	Corresponding feature of optical data[b,c]	Present assignment	Earlier assignment
6.6	P1	5.3	−1.3	Direct	6.8 (E_1')	Zone edge near W-K	$L_{3v} \rightarrow L_{3c}$
~7.2	P2	~6.2	~−1.0	Direct	7.6 ($E_1'+\Delta_1$)	Direct transition	$L_{3v} \rightarrow L_{3c}$
8.0	P2	6.2	−1.8	Nondirect	8.0[c]	Coupling of peaks in density of states	$L_{3v} \rightarrow L_{3c}$
5.8	S1	5.8	0.0	Direct	5.8	$\Gamma_{15v} \rightarrow \Gamma_{15c}$	$X_{5v} \rightarrow X_{3c}$
8.7	S2	8.2[d]	−0.5	Direct	d_1 beginning near 8.7 eV	$\Gamma_{15v} \rightarrow \Gamma_{1c}$	Threshold of d-band transitions
≳8.0	P3	$\hbar\omega-1.9$	−1.9	Nondirect		Peak in valence band density of states	
≳9.3	P4	$0.5\,\hbar\omega+2.5$	$-0.5\,\hbar\omega+2.5$	Direct		Near Σ and Δ axes	
≲8.5	P5	6.9					
	D		−10.3		14 (d_2)	Transitions from d band	Transitions from d band

[a] Energies are given in electron volts above the valence-band maximum. The estimated uncertainty in the location of peaks in the NEDC is ±0.2 eV.
[b] Reference 3.
[c] Reference 21.
[d] The motion of S2 with increasing photon energy is discussed in Secs. IV and VI.

states for P4 are in the second valence band[29] which extends from $-3.5 \lesssim E < 0$ eV. We note from the NEDC (Fig. 16) and Eq. (2) that for $\hbar\omega = 11.8$ eV the initial states for P4 are at -3.4 eV, close to the lower limits of the valence band located by the disappearance of P1 (Fig. 4) and P5 (Fig. 15), and that the final states are near 8.4 eV. Figure 24 suggests that the states leading to P4 lie near the Σ and Δ directions and that P4 is moving toward the X point as the photon energy is increased.

In Table IV we summarize the structure observed in the NEDC. We include the assignments suggested by this work as well as earlier assignments.

VII. CONCLUSIONS

We have shown that the structure in the photoemission from CdTe results from a mixture of direct and nondirect transitions. By correlating structure in the energy distributions of the photoemitted electrons with structure in the optical data, we determine the absolute energies of the initial and final states for the transitions associated with structure in the optical data. These data are summarized in Table IV.

When structure in the optical and photoemission data is due to direct transitions, the photoemission data provide a measurement of the energies of specific levels in the band structure. In this way we have determined the energies of Γ_{15c}, Γ_{1c}, and the uppermost valence band and second conduction band along the zone edge between W and K. In addition we find weaker direct transitions probably associated with the Λ direction. We have used the density-of-states analysis to determine the effective density of states causing the nondirect contributions to the NEDC. The nondirect transitions observed in the photoemission data are due principally to a peak at -1.9 eV in the valence-band density of states and a gentle peak at 6.2 eV in the conduction-band density of states. We find that the valence band is about 3.7 eV wide in reasonable agreement with band theory.

APPENDIX: DENSITY-OF-STATES ANALYSIS

1. Energy Distribution Predicted by Nondirect Model

The energy distributions of the photoemitted electrons (NEDC) differ from the energy distributions of the photoexcited electrons due to scattering processes and the potential barrier at the surface. Here we derive the expression for the NEDC predicted by the nondirect model; in part 2 we present the details of the density-of-states analysis[12] and give a simple example.

The nondirect model assumes that the strength of an electronic transition is proportional to the product of the initial and final densities of states. The matrix elements coupling initial and final states are assumed equal to a constant for all transitions conserving energy and zero otherwise. On this model the energy distribution of the photoexcited electrons per absorbed photon, i.e., the normalized distribution, is

$$n(E,\hbar\omega) = \frac{N_c(E)N_v(E-\hbar\omega)}{\int_{E_g}^{\hbar\omega} N_c(E)N_v(E-\hbar\omega)dE}, \qquad \text{(A1)}$$

where N_v and N_c are the valence-band and conduction-band densities of states.

The energy distribution of the photoemitted electrons (NEDC) differs from the energy distribution of the photoexcited electrons Eq. (A1), for the reasons given above. If the surface of the solid is planar and if there is no scattering, then only half of the photoexcited electrons are initially heading toward the surface. Furthermore, the threshold function (or surface transmission probability), $T(E)$, is the probability that an electron reaching the surface with energy E will escape the solid. For energies below the vacuum level, $T(E)=0$; for energies above the vacuum level it is expected that $T(E)$ will be a smooth function of energy.

Corrections to Eq. (A1) due to electron-electron scattering of electrons out of the energy distributions can be approximated. It is assumed[19] that $e^{-x/L(E)}$ is the probability that an electron excited to an energy E at a distance x from the surface will travel to the surface without suffering an inelastic collision. We refer to $L(E)$ as the escape depth for electrons at energy E. At a distance x from the surface the intensity of radiation is proportional to $e^{-\alpha x}$, where $\alpha(\hbar\omega)$ is the absorption coefficient for a photon energy $\hbar\omega$. If α is much larger than $1/L$, most of the absorption is within an escape depth of the surface and relatively few electrons are inelastically scattered on their way to the surface; if α is much smaller than $1/L$, light reaches far into the crystal and there is a large probability that an electron will be scattered before it reaches the surface. It is readily shown[19] that the fraction of electrons excited to an energy E that reach the surface without scattering is

$$S(E,\hbar\omega) = \frac{\alpha(\hbar\omega)L(E)}{1+\alpha(\hbar\omega)L(E)}. \qquad \text{(A2)}$$

If all scattered electrons are unable to escape the solid (i.e., are electron-electron scattered to energies below the vacuum level), the energy distribution of the photoemitted electrons is given by

$$n(E,\hbar\omega) = \frac{T(E)S(E,\hbar\omega)N_c(E)N_v(E-\hbar\omega)}{2\int_{E_g}^{\hbar\omega} N_c(E)N_v(E-\hbar\omega)dE}. \qquad \text{(A3)}$$

Since the minimum energy loss through electron-electron scattering is equal to the band gap, and the more probable energy losses exceed the band gap, Eq. (A3) is a reasonable treatment of electron-electron

[29] The valence bands are numbered in order of increasing energy. Bands 2, 3, and 4 appear in Fig. 24.

scattering, at least for photon energies within about a band gap above the threshold for photoemission.

In the derivation of Eq. (A3) we have ignored all effects due to phonon scattering. For the cases of interest here, photoemitted electrons are sufficiently energetic that electron-electron scattering can be expected to provide the dominant energy loss mechanism. Furthermore, we showed in Sec. IV that none of the transport effects suggested by Kane[20] are observed in the CdTe photoemission data. However, as discussed previously, low-energy peaks appearing at higher-photon energies are produced by the pair-production scattering event.

For the nondirect model of electronic excitation, the imaginary part of the dielectric function ϵ_2 is simply related[5] to the denominator in Eq. (A3)

$$\epsilon_2 = A\int_{E_g}^{\hbar\omega} \frac{N_c(E)N_v(E-\hbar\omega)dE}{\omega^2}, \tag{A4}$$

where A is an undetermined constant. Also, on the basis of photoemission data alone, the product $T(E)N_c(E)$ cannot be resolved into the two distinct quantities. We therefore define this product as the effective conduction-band density of states $N_c^{\text{eff}}(E)$. Substituting Eq. (A4) into (A3) and introducing $N_c^{\text{eff}}(E)$ we have

$$n(E,\hbar\omega) = \frac{AS(E,\hbar\omega)N_c^{\text{eff}}(E)N_c(E-\hbar\omega)}{2\omega^2\epsilon_2}. \tag{A5}$$

Finally, we combine terms to form a correction term

$$C(E,\hbar\omega) = \frac{AS(E,\hbar\omega)}{2\epsilon_2\omega^2}, \tag{A6}$$

so that the energy distribution of the photoemitted electrons (NEDC) is given by

$$n(E,\hbar\omega) = C(E,\hbar\omega)N_c^{\text{eff}}(E)N_v(E-\hbar\omega). \tag{A7}$$

We now discuss two approximations for $C(E,\hbar\omega)$ which are used since we cannot reliably estimate the energy dependence of the escape depth $L(E)$. When $\alpha L \gg 1$, the escape depth is long compared to the absorption depth $(1/\alpha)$ so that most electrons reach the surface without scattering. Then $S(E,\hbar\omega)\approx 1$ and $C(E,\hbar\omega) \propto 1/(\epsilon_2\omega^2)$. Using published optical data for ϵ_2, $C(E,\hbar\omega)$ is determined and Eq. (A7) reduces to

$$n(E,\hbar\omega) \propto \frac{N_c^{\text{eff}}(E)N_v(E-\hbar\omega)}{\epsilon_2\omega^2}. \tag{A8}$$

The second limiting form is used when $\alpha L \ll 1$. For this case the escape depth is short compared to the absorption depth so that most electrons are electron-electron scattered before they reach the surface. Then $S(E,\hbar\omega) \approx \alpha L$ and $C(E,\hbar\omega) \propto \alpha L/(\epsilon_2\omega^2) \propto L/(n_0\omega)$. The refractive index n_0 is available from published optical data, but we cannot reliably estimate $L(E)$. We therefore include $L(E)$ in the effective conduction-band density of states and Eq. (A7) reduces to

$$n(E,\hbar\omega) \propto \frac{N_c^{\text{eff}'}(E)N_v(E-\hbar\omega)}{n_0\omega}, \tag{A9}$$

where $N_c^{\text{eff}'}(E) \equiv L(E)T(E)N_c(E)$.

2. Theory of Density-of-States Analysis

We shall describe the density-of-states analysis using Eq. (A9) which is valid when $\alpha L \ll 1$. If $\alpha L \gg 1$, then the energy distributions are given by Eq. (A8) and the analysis which follows must be modified by replacing $n_0\omega$ by $\epsilon_2\omega^2$. The low yield (1–10 percent) measured at photon energies when all final states are above the vacuum level indicates that most electrons are electron-electron scattered before they reach the surface; hence $\alpha L \ll 1$ and Eq. (A9) applies. A knowledge of the absolute yield and the absorption coefficient allows us to estimate the escape depth for the high-vacuum-cleaved sample. It is apparent from Figs. 21 and 22 that for $\hbar\omega > 10$ eV most of the absorption is to final states well above the vacuum level. It follows from Eq. (A2) that the yield is approximately

$$Y \approx \frac{0.5\alpha LT}{1+\alpha L}. \tag{A10}$$

In Eq. (A10), L is an average escape depth. This form will suffice here even though Spicer[19] has given an exact expression for the appropriate average over the escape depths of the photoemitted electrons. For $\hbar\omega = 10.2$ eV, $Y = 0.035$ (Fig. 1) and if we assume that $T \approx 0.25$, then $\alpha L = 0.39$. Using an absorption coefficient[30] of 9.5×10^5 cm^{-1}, we find that the escape depth is about 41 Å for electrons about 8.5 eV above the valence-band maximum.

The density of states analysis determines the valence-band density of states in the following manner. If we choose a fixed final-state energy $E = E_f$, then in Eq. (A9), $N_c^{\text{eff}'}(E_f)$ is a constant. For a photon energy $\hbar\omega$, the valence-band density of states at an energy $E_f - \hbar\omega$ is proportional to the amplitude of the NEDC at an energy E_f, and to $n_0\omega$:

$$N_v(E_f-\hbar\omega) \propto \frac{n_0\omega}{N_c^{\text{eff}'}(E_f)} n(E_f,\hbar\omega). \tag{A11}$$

In other words, the amplitudes of the NEDC at only one energy E_f but for all photon energies suffice to determine the relative valence-band density of states seen by a final-state energy E_f. If we choose another final energy E_f, the relative valence-band density of states can again be determined. In general the valence-band densities of states computed in this manner will not superimpose for different final states since the

[30] M. Cardona, J. Appl. Phys. 36, 2181 (1965).

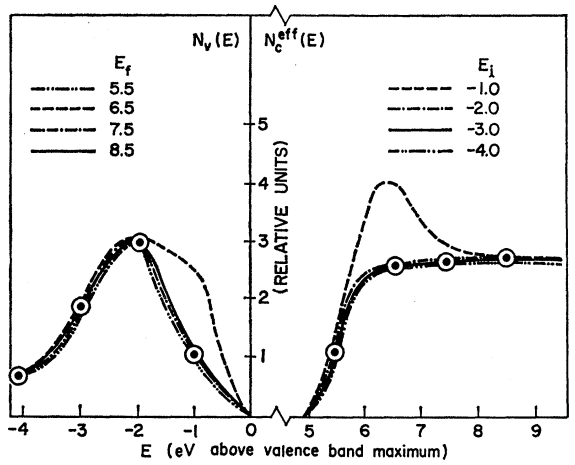

FIG. 26. Example of density-of-states analysis of typical photoemission data. E_f is the energy of the conduction-band state used to derive the valence-band density of states $N_v(E)$; E_i is the energy of the initial state used to derive the effective conduction-band density of states $N_c^{eff}(E)$. The points indicate the values used in Eqs. (A11) and (A12).

NEDC [Eq. (A9)] is also proportional to the effective conduction-band density of states $N_c^{eff'}(E)$. The scale factors $1/N_c^{eff'}(E)$ are determined by making the computed valence-band densities of states superimpose. The resulting $N_c^{eff'}(E_f)$ is the effective conduction-band density of states. If the valence-band densities of states seen by all final states superimpose, one must conclude that the nondirect model is sufficient to completely explain the photoemission data.

If the shapes of the valence-band densities of states seen by any two final states differ, one must conclude that the nondirect model is not sufficient to explain the photoemission data. Although a unique density of states cannot be determined, the general features of the valence-band density of states (peaks, dips, etc.) are apparent when one compares the valence-band densities of states seen by various E_f.

The density-of-states analysis determines the conduction-band density of states in the following manner. If we choose a fixed initial state energy $E_i=E-\hbar\omega$, then in Eq. (A9) $N_v(E_i)$ is a constant. For a photon energy $\hbar\omega$, the effective conduction-band density of states at an energy $E_i+\hbar\omega$ is proportional to the amplitude of the NEDC at an energy $E_i+\hbar\omega$ and to $n_0\omega$

$$N_c^{eff'}(E_i+\hbar\omega) \propto \frac{n_0\omega}{N_v(E_i)} n(E_i+\hbar\omega,\hbar\omega), \quad \text{(A12)}$$

where $N_v(E_i)$ is a constant. In other words, the amplitudes of the NEDC at an energy $\hbar\omega$ above one initial energy but for all photon energies suffice to determine the relative conduction-band density of states. If we choose another initial energy E_i, the relative conduction-band density of states can again be determined. In general, the effective conduction-band densities of states computed in this manner will not superimpose for different initial-state energies since the NEDC [Eq. (A9)] is also proportional to the effective valence-band density of states $N_v(E_i)$. The scale factors $1/N_v(E_i)$ are determined by making the effective conduction-band densities of states superimpose. The resulting $N_v(E_i)$ is is the valence-band density of states. If the effective conduction-band densities of states seen by all initial states superimpose, one must conclude that the nondirect model is sufficient to explain the photoemission data.

The test for the validity of the nondirect model is therefore very simple and straightforward. One attempts to derive the valence-band and conduction-band effective densities of states from the photoemission data. The results must be consistent in that the densities of states derived using various initial and final states must be the same. If the curves superimpose, one must conclude that the density-of-states model is sufficient to explain the photoemission data. On the other hand, if the densities of states do not superimpose, one must conclude that the density of states model is not sufficient to explain the photoemission data. The amount by which the curves do not superimpose is a quantitative measure of the matrix element variation required to explain the photoemission data.

We now give a simple example of the density of states analysis showing the effects of the simultaneous presence of direct and nondirect transitions. We show in Fig. 26 the valence-band and conduction-band effective densities of states which might result from the density of states analysis of a typical set of photoemission data. The circles indicate the scale factors used in Eqs. (A11) and (A12). E_f is the final-state energy used to derive the valence-band density of states; E_i is the initial-state energy used to derive the effective conduction-band density of states.

Since most of the curves in Fig. 26 superimpose, the nondirect model explains most of the photoemission data. However, the effective conduction-band density of states seen by $E_i=-1.0$ eV lies above the other densities of states for $E\approx 6.5$ eV, and the valence-band density of states seen by $E_f=6.5$ eV lies above the other densities of states for $E\approx -1.0$ eV. This indicates that transitions from initial states near -1.0 eV to final states near 6.5 eV are stronger than the nondirect model predicts. About half of the electrons excited from initial states near -1.0 eV to final states near 6.5 eV result from direct transitions.

Note added in proof. Professor Marvin Cohen has independently recognized that the regions of the Brillouin zone near W and K are important in the II–VI compounds (private communication).

ACKNOWLEDGMENTS

The authors are grateful to Dr. Frank Herman and Professor Marvin Cohen for many helpful comments.